Activation of Peroxymonosulfate Using Secondary Pyrolysis Oil-Based Drilling Cuttings Ash for Pollutant Removal

Yuqing Zhao, Hang Yang, Jianfa Sun, Yi Zhang,* and Shibin Xia*

ACCESS | Metrics & More | Article Recommendations

ABSTRACT: In this study, the utilization of secondary pyrolysis oil-based drilling cuttings ash (OBDCA-sp) to activate peroxymonosulfate (PMS) for pollutant removal was investigated. The chemical and physical properties of OBDCA-sp were explicitly analyzed via multiple characterization. The activation efficiency of OBDCA-sp for PMS was tested using humic acid (HA) as the target pollutant. 92% of HA and 52% of total organic carbon in solution could be removed using OBDCA-sp-activated PMS under optimal conditions: OBDCA-sp dosage at 4 g/L, PMS concentration at 4 mmol/L, HA concentration at 10 mg/L, and pH value at 7. After four cycles, 84% removal rate of HA could still be achieved using OBDCA-sp to activate PMS. The main catalysis elements for PMS activation in OBDCA were postulated to be Fe(III), Co(III), and Mn(III), based on X-ray photoelectron spectroscopy and X-ray diffraction results. The results of the quenching experiment indicated that $SO_4^{\bullet-}$, $^\bullet OH$, and $^1O_2$ were the main reactive oxygen species (ROS) and that $^1O_2$ was the dominant ROS in the HA removal process. Radical trapping experiments indicated the presence of $SO_4^{\bullet-}$, $^\bullet OH$, and $^1O_2$ in the reaction system. This study presented a novel utilization path of OBDCA in the field of environmental remediation.
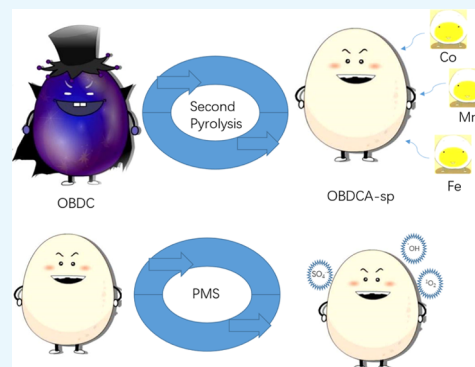
1. INTRODUCTION

In China, oil-based drilling cuttings (OBDCs) are classified as a hazardous waste, which is mainly derived from the process of crude oil development and extraction.[1,2] OBDC has a complex composition, including oil−water mixtures, heavy metals, soil components, and various surfactants.[3] The discharge of untreated/inappropriately treated OBDC could cause severe adverse impact on the surrounding environment.[4] At present, many treatment strategies for OBDC have been studied, including pyrolysis, oxidation, microbial treatment, and solvent extraction.[5−8]

Pyrolysis is the most common treatment method for OBDC due to its advantages of high scalability, ease of operation, and relatively low cost. Large amounts of OBDC ash (OBDCA) are produced as the pyrolysis product of OBDC, which are industry pain points and should be further utilized. Usually, OBDCA was employed as a raw material for bricks, cement, and proppants.[9−11] Nowadays, OBDCA is rarely used in the field of environmental remediation. In our previous study, OBDCA was used as an environment-friendly material for treating Cr(VI)-contaminated soil and water.[12,13] There are only rare studies about the use of OBDCA for organic pollutant removal.

Persulfate activation is an important advanced oxidized technology that can rapidly and efficiently degrade organic pollutants in an environment without causing secondary pollution.[14−16] Persulfate activation includes peroxymonosul-

fate and peroxydisulfate activation. Transition metals, especially Fe, Co, and Mn, are the most common persulfate catalysts.[17−20] Interestingly, OBDCA is composed of complex composition, which contains certain transition metals. Therefore, it is interesting to explore whether OBDCA can potentially be used to activate persulfate for organic pollutant removal.

Humic acid (HA) is a common natural organic substance in natural water bodies. The presence of excessive HA could cause some adverse impact on the environment. For water bodies, HA could result in changes in color and produce unpleasant odors.[21] It is reported that the accumulation of HA may cause the clogging of constructed wetlands.[22] In the chlorine disinfection process, the presence of HA will produce some carcinogenic byproducts.[23] In addition, HA has adsorption and complexation effects on some organics and heavy metals in the environment, which is not conducive to the removal of other pollutants.[24] Therefore, the removal of HA in the water body is of significant importance, which can improve

the quality of the water body and reduce the migration and conversion of pollutants.

The aim of this paper is to: (1) study the efficiency of removal of HA using OBDCA-activated peroxymonosulfate (PMS); (2) investigate the effect of different experimental conditions of PMS activation on HA removal; (3) analyze the reusable performance of OBDCA and the main reactive oxygen species (ROS) produced in PMS activation; and (4) characterize fresh and used OBDC using X-ray diffraction (XRD) and X-ray photoelectron spectroscopy (XPS).

2. EXPERIMENTAL SECTION

2.1. Chemicals and Reagents. The chemicals and reagents used in this study were of analytical grade and used as received without further purification. OBDCA was provided by the Agriculture and Forestry Department of Fuling Shale Gas Company. HA was obtained from the International Humic Acid Association. Peroxymonosulfate, sulfuric acid, sodium hydroxide, tert-butanol (TBA), ethanol (EtOH), dimethyl pyridine N-oxide (DMPO), 2,2,6,6-tetramethylpiperidine-1-oxyl (TEMPO), phenyl methyl sulfoxide (PMSO), and tryptophan were purchased from Aladdin Company. The stock solutions of HA (100 mg/L) and PMS (100 mg/L) were prepared using ultrapure water.

2.2. Secondary Pyrolysis Procedure for OBDC. Secondary pyrolysis was used to remove the residual organic matter in OBDCA. According to our previous study, a modified pyrolysis procedure was employed.[13] In brief, the secondary pyrolysis of OBDCA was conducted in a muffle at 750 °C for 90 min at a heating rate of 6 °C/min under N_2 atmosphere. The secondary pyrolysis product of OBDCA was abbreviated as OBDCA-sp.

2.3. Experimental Work. A certain amount of OBDCA-sp and 100 mL of HA aqueous solution were added to a flask. The pH of the solution was adjusted using 1 mol/L H_2SO_4 and 1 mol/L NaOH. Then, the flask was put in a shaker to conduct experiments at 200 rpm and 25 °C. At predetermined time intervals, 5 mL of the solution was withdrawn and filtered using a syringe filter, and the concentration of HA was measured using an UV spectrometer at 254 nm.

2.4. Analysis for OBDCA and HA Solution. The crystalline structures of OBDCA-sp were analyzed using an X-ray diffractometer (D8 Advance). The surface compositions and oxidation states of OBDCA-sp were analyzed using an X-ray photoelectron spectrometer (EscaLab Xi+). The morphology of OBDCA-sp was identified using a scanning electron microscope (JSM-IT300) and a transmission electron microscope (Tecnai F20). The surface area and pore volume were analyzed using a Brunauer–Emmett–Teller (BET) surface area analyzer (Mike 2020). The zeta potential of OBDCA-sp was analyzed using a zeta potential analyzer (ZetaPALS). Electronic paramagnetic resonance (EPR/ESR, Brook A300) was used to capture the radicals produced in solution. The leaching concentration was analyzed using an inductively coupled plasma mass spectrometry (ICP−MS, PerkinElmer) system. An X-ray fluorescence spectrometer (PANalytical Axios) was used to analyze the fluorescence spectroscopic measurements (excitation−emission matrix, EEM). A UV−vis spectrophotometer (UNICOWFUV-2) and a TOC analyzer were used to analyze the HA solution. A shaker (SHZ-2A) was used throughout the experiment. The removal rate of HA was calculated according to eq 1

$$\text{Removal rate} = \frac{C_0 - C_t}{C_0} \tag{1}$$

where C_t is the HA concentration at time t (mg/L), and C_0 is the initial HA concentration (mg/L).

3. RESULTS AND DISCUSSION

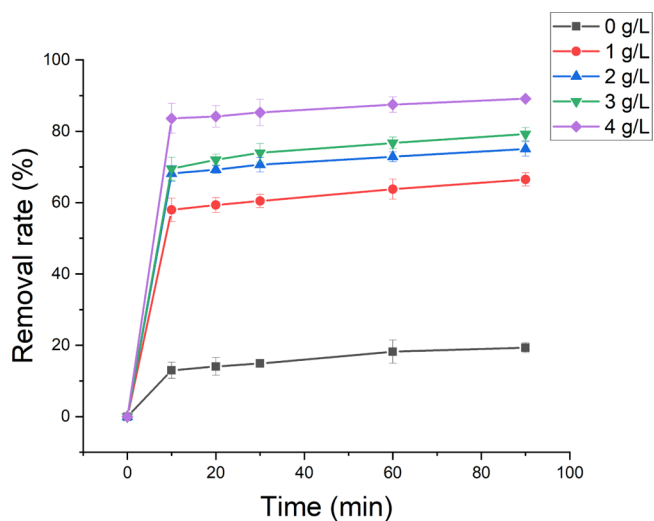**3.1. Effect of the Dosage of OBDCA-sp on HA Removal.** Figure 1 shows the effect of OBDCA-sp dosage

Figure 1. Effect of different dosages of OBDCA-sp on HA removal. Experimental parameters: dosage of OBDCA-sp: 0–4 g/L; PMS: 1 mmol/L; HA: 10 mg/L; pH: 7.
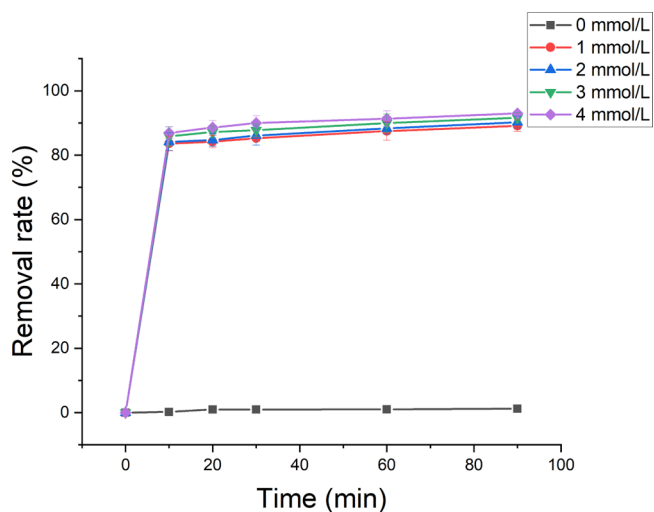

Figure 2. Effect of PMS concentration on HA removal. Experimental parameters: dosage of OBDCA-sp: 0.4 g/L; PMS: 0−4 mmol/L; HA: 10 mg/L; pH: 7.

on HA removal. The removal rate of HA increased with the increasing dosage of OBDCA-sp from 0 to 4 g/L. With no addition of OBDCA-sp, the removal rate of HA reached 19% after 90 min of reaction, which was ascribed to the directly oxidized HA in solution by PMS. When the dosage of OBDCA-sp was 4 g/L, the removal rate of HA reached 89% after 90 min of reaction. A higher dosage of OBDCA-sp could provide more active sites to activate PMS and produce more ROS. However, excessive dosage of OBDCA-sp increased the
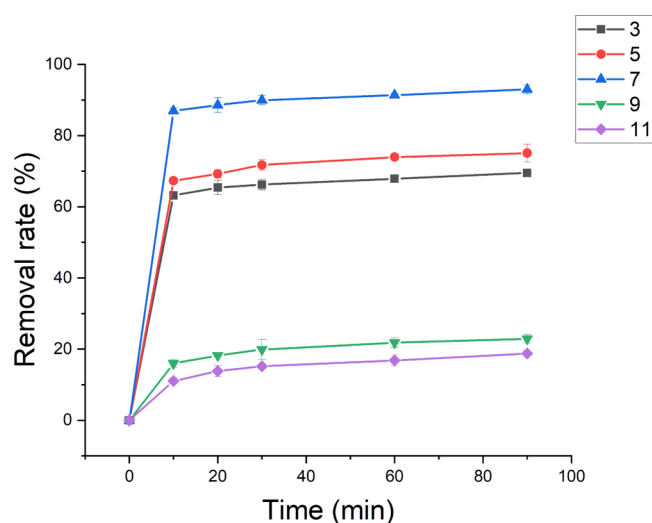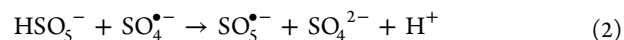
Figure 3. Effect of pH on HA removal. Experimental parameters: OBDCA-sp: 4 g/L dosage; PMS: 4 mmol/L; HA: 10 mg/L; pH: 3–11.

cost and may also cause the blockage of active sites, which was not conducive to the removal of HA. Therefore, the dosage of OBDCA-sp in the subsequent experiments was set as 4 g/L.

3.2. Effect of PMS Concentration on HA Removal. Figure 2 shows the effect of PMS concentration on the removal of HA. The concentration of PMS increased from 0 to 4 mmol/L. With no addition of PMS, the removal of HA was very low (<1%), which indicated the poor and neglected adsorption of HA on OBDCA-sp. The removal rate of HA slightly increased with the increasing PMS concentration.

When the PMS concentration was 4 mmol/L, the removal rate of HA reached 92% after 90 min of reaction. The poor effect from the increased PMS concentration for HA removal was due to the following reasons: (i) although a higher concentration of PMS in the solution could produce more ROS during the activation process, according to formula 2, PMS was one of the scavengers of $SO_4^{\bullet-}$, which was not conducive to HA removal;[25] (ii) due to the limitation of the catalyst (OBDCA-sp) quantity, it could provide only limited active sites for PMS activation, resulting in the incomplete activation of excessive PMS.[26] To achieve the maximum HA removal, the PMS concentration in the subsequent experiments was set as 4 mmol/L.

$$HSO_5^- + SO_4^{\bullet-} \rightarrow SO_5^{\bullet-} + SO_4^{2-} + H^+ \qquad (2)$$

3.3. Effect of pH on HA Removal. Figure 3 shows the effect of pH on the removal of HA. The removal rate of HA decreased as the solution changed from neutral to acidic or alkaline. When the pH of the solution was 3, the removal rate of HA reached 69.5% after 90 min of the reaction; when the pH of the solution was 11, the removal rate of HA reached 18.7% after 90 min of the reaction. The results indicated that both acidic and alkaline solutions were not conducive to the removal of HA. PMS existed in different forms in solution at different pH (pK_{a1} of PMS <0, and pK_{a2} of PMS = 9.4).[27] Under acidic conditions, the main forms of PMS in the solution were HSO_5^- and SO_4^{2-}; in neutral solutions, the main form of PMS in the solution was HSO_5^-; while in alkaline solutions, according to formula 3, the main form of PMS in solution was SO_5^{2-}.[28,29] The pK_a value of OBDCA-sp was calculated as 2.01, indicating that when the pH of the solution was less than 2.01, the surface of OBDCA-sp in the
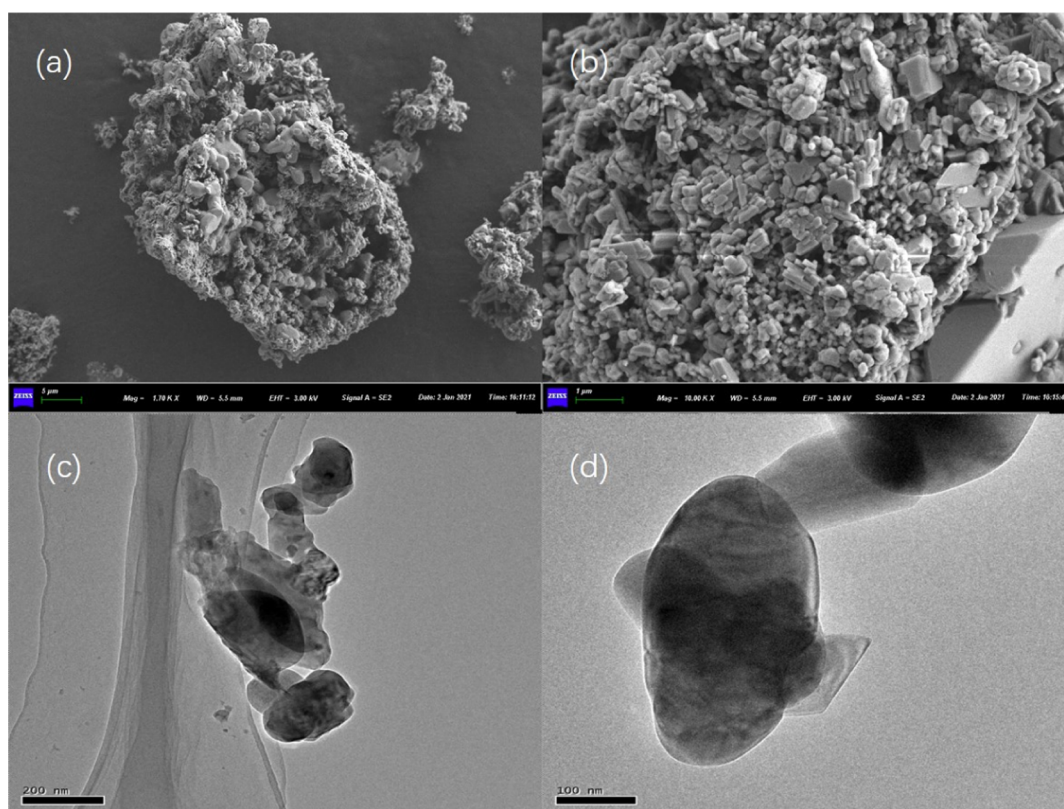

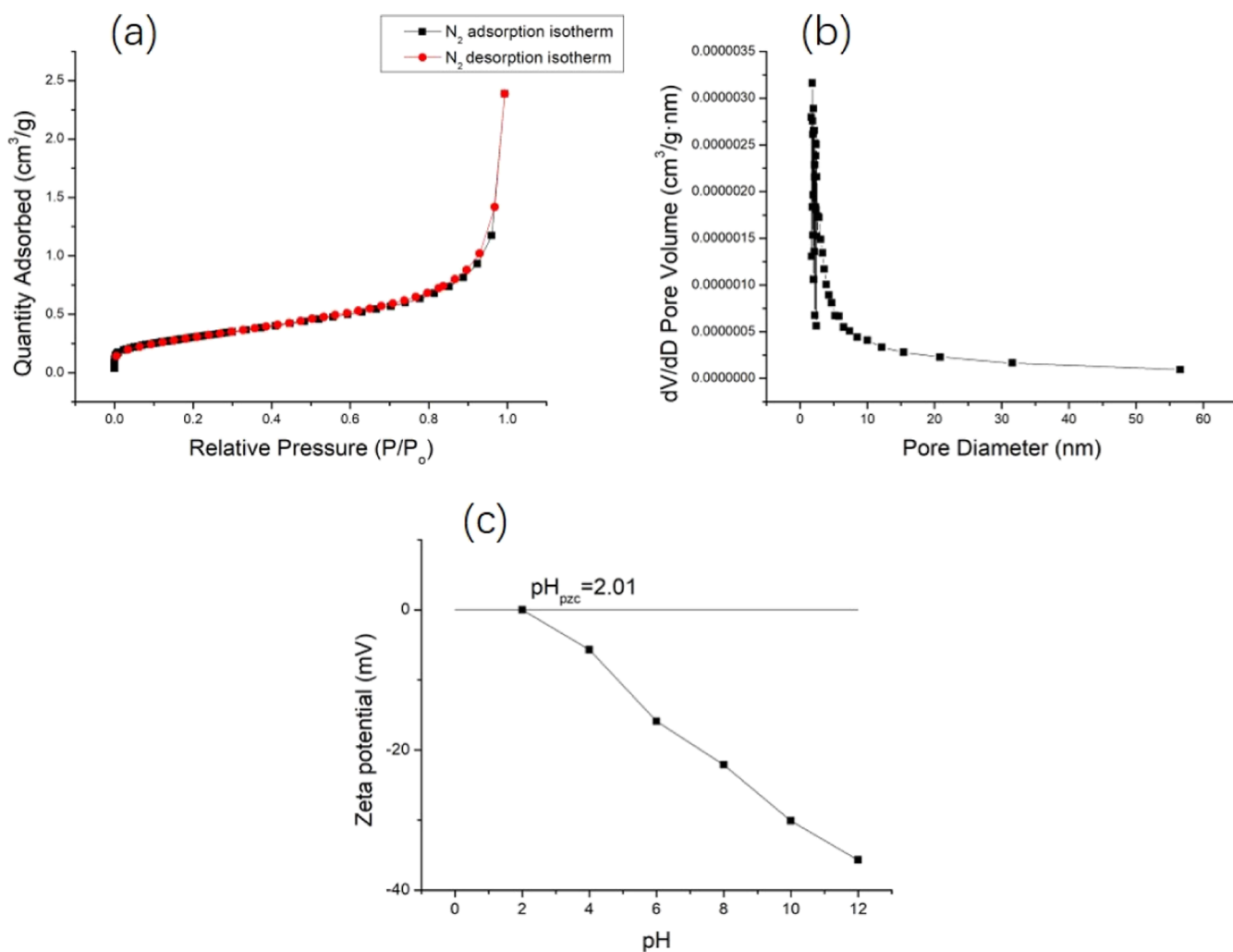**Figure 4.** (a,b) SEM image of OBDCA-sp; (c,d) TEM image of OBDCA-sp.

Figure 5. (a) Nitrogen adsorption−desorption isotherms, (b) pore distribution of OBDCA-sp, and (c) zeta potential analysis for OBDCA-sp.

Table 1. BET Parameters for OBDCA-sp

specific area (m^2/g)	volume (cm^3/g)	average pore diameter (nm)	average particle diameter (nm)
1.0993	0.0013	5.01	5458.25

solution was positively charged, and when the pH of the solution was greater than 2.01, the surface of OBDCA-sp in the solution was negatively charged. Therefore, the reasons for the poor removal effect of HA under acidic conditions were: (i) the complexation reaction of HA to the metal on the surface of OBDCA-sp; (ii) according to formula 4, the generated $SO_4^{\bullet-}$ may be changed to form $^{\bullet}OH$.[30] The reasons for the poor removal effect of HA under alkaline conditions were : according to formula 5, OH^- was also the scavenger of $SO_4^{\bullet-}$, forming $^{\bullet}OH$ with a lower redox potential;[31] (ii) according to the above dissociation coefficient, the surface of OBDCA-sp had a significant electrostatic mutual repulsion effect with SO_5^{2-}, resulting in a decrease in the HA removal effect; (iii) in addition, the main composite of OBDCA-sp was SiO_2, which could be dissolved in alkaline conditions and was not conductive to the activation of PMS. Therefore, in the subsequent experiments, the pH value in the solution was adjusted to 7.
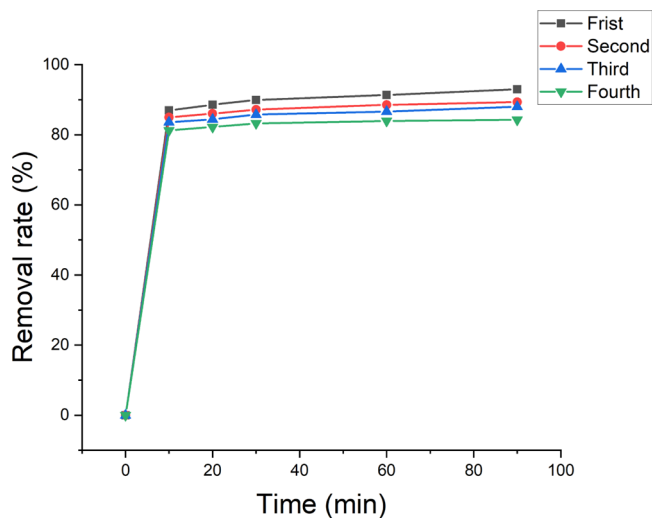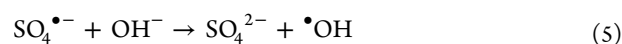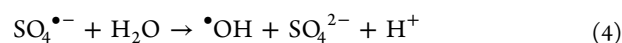
$$HSO_5^- \rightarrow SO_5^{2-} + H^+ \qquad (3)$$

Figure 6. Cycle utilization of OBDCA-sp. Experimental parameters: OBDCA-sp: 4 g/L dosage; PMS:4 mmol/L; HA: 10 mg/L; pH: 7.

$$SO_4^{\bullet-} + H_2O \rightarrow {}^{\bullet}OH + SO_4^{2-} + H^+ \qquad (4)$$

$$SO_4^{\bullet-} + OH^- \rightarrow SO_4^{2-} + {}^{\bullet}OH \qquad (5)$$
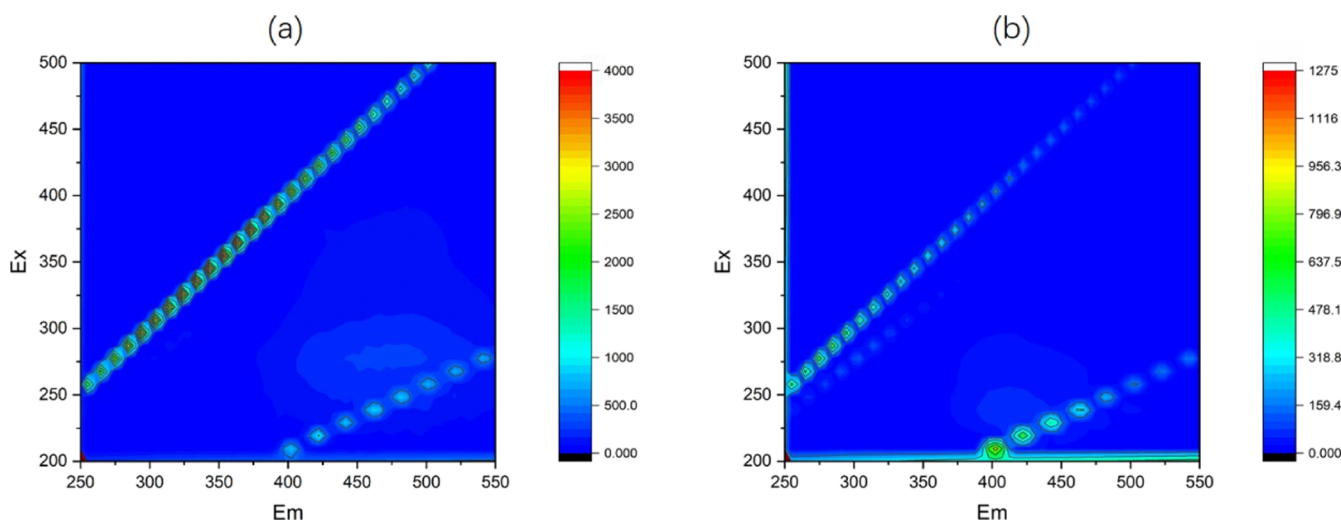
Figure 7. (a) EEM of HA solution and (b) EEM of treated HA solution. Experimental parameters: OBDCA-sp: 4 g/L dosage; PMS:4 mmol/L; HA: 10 mg/L; pH: 7.

Table 2. Leachate Concentration of OBDCA-sp

element	concentration (mg/L)
Co	0.0001
Cr	0.0062
Fe	0.0036
Mn	0.0043

3.4. Morphology, BET, and Surface Potential Analyses of OBDCA-sp. The morphology analysis of OBDCA-sp was observed using SEM and TEM (Figure 4). OBDCA-sp was irregularly shaped with a coarse surface covered by corundum-like crushed particles. The BET and zeta potential analyses of OBDCA-sp were also carried out (Figure 5). The N_2 adsorption/desorption isotherms for OBDCA-sp were classified as type III with H3 hysteresis, loops based on the Brunauer−Deming−Deming−Teller classification, which in-

dicated that the surface of OBDCA-sp exhibited a slit hole formed by the accumulation of flake particles. The specific surface area and pore volume of OBDCA-sp (Table 1) were 1.09 m^2/g and 0.0013 cm^3/g, respectively. The pHpzc value of OBDCA-sp was obtained according to the calculation of zeta potentials, which indicated that the surface charge of OBDCA-sp was negative, with the pH exceeding 2.01.

3.5. Recycled Utilization and Characterization of OBDCA-sp for HA Solution. The recycled utilization of OBDCA-sp to activate PMS for HA removal was tested (Figure 6). After four rounds of recycling, 84% HA removal rate could still be achieved using OBDCA to activate PMS. The reduced removal efficiency was owing to the weight loss of OBDCA-sp. The HA solution before and after the reaction was measured using EEM (Figure 7), which evidently indicated the removal of HA in the characteristic regions (λ_{ex} = 200−250
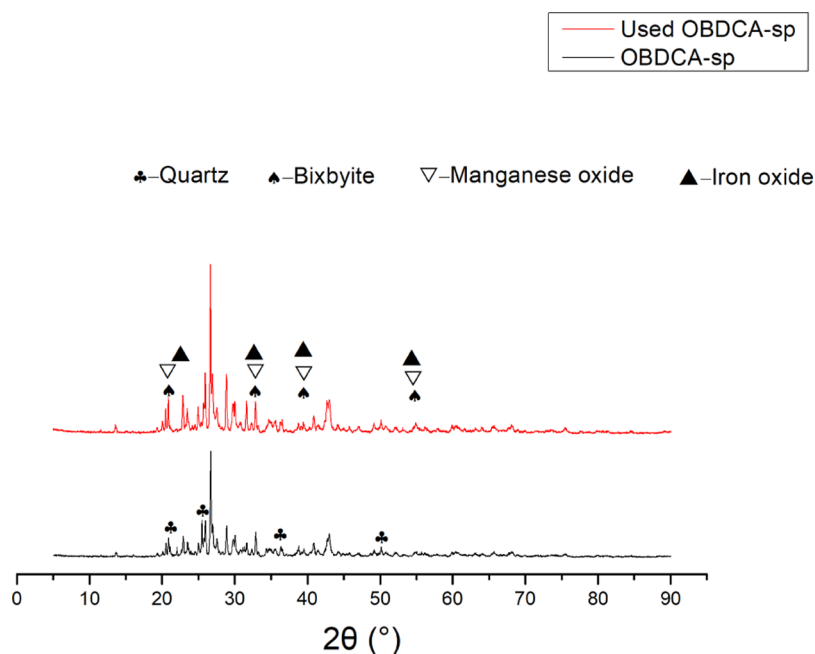

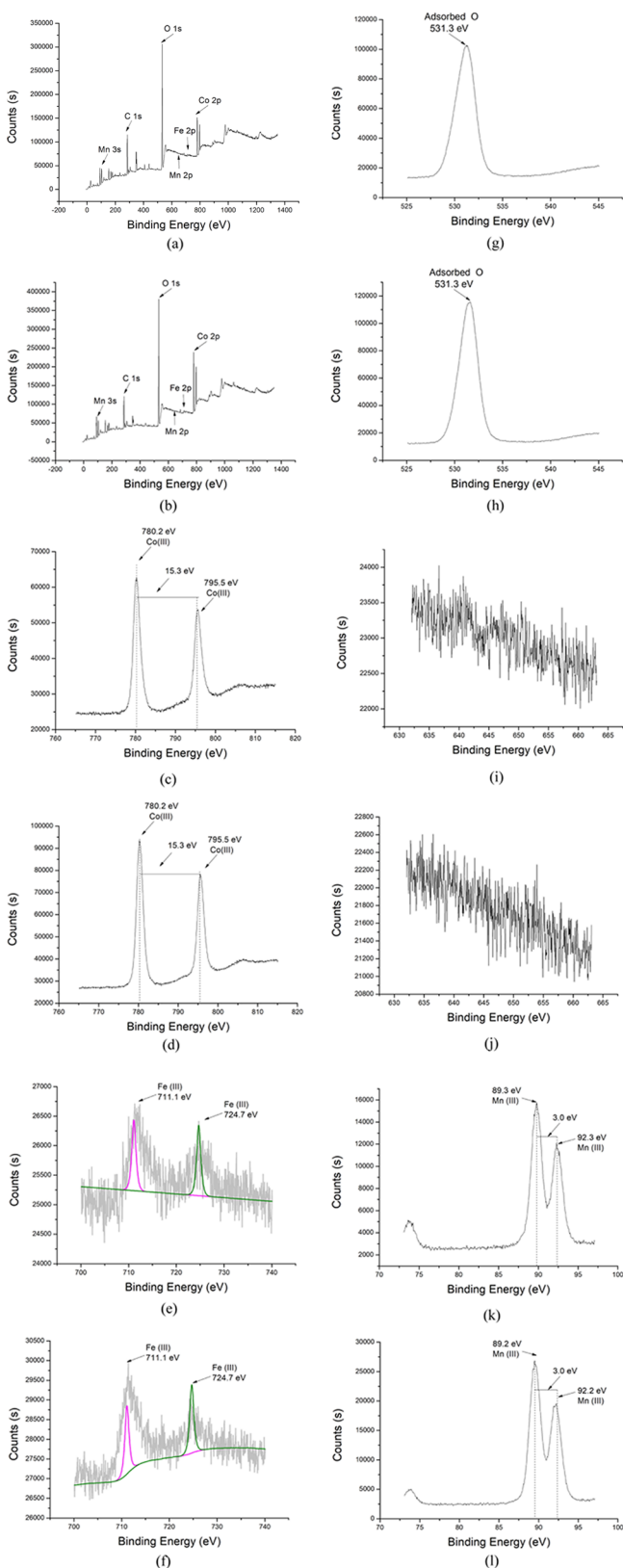**Figure 8.** XRD pattern of OBDCA-sp.

Figure 9. XPS analysis of OBDCA-sp with (a) survey of original OBDCA-sp, (b) survey of used OBDCA-sp, (c) Co 2p of original OBDCA-sp, (d) Co 2p of used OBDCA-sp, (e) Fe 2p of original OBDCA-sp, (f) Fe 2p of used OBDCA-sp, (g) O 1s of original OBDCA-sp, (h) O 1s of used OBDCA-sp, (i) Mn 2p of original OBDCA-sp, (j) Mn 2p of used OBDCA-sp, (k) Mn 3s of original OBDCA-sp, and (l) Mn 3s of used OBDCA-sp.
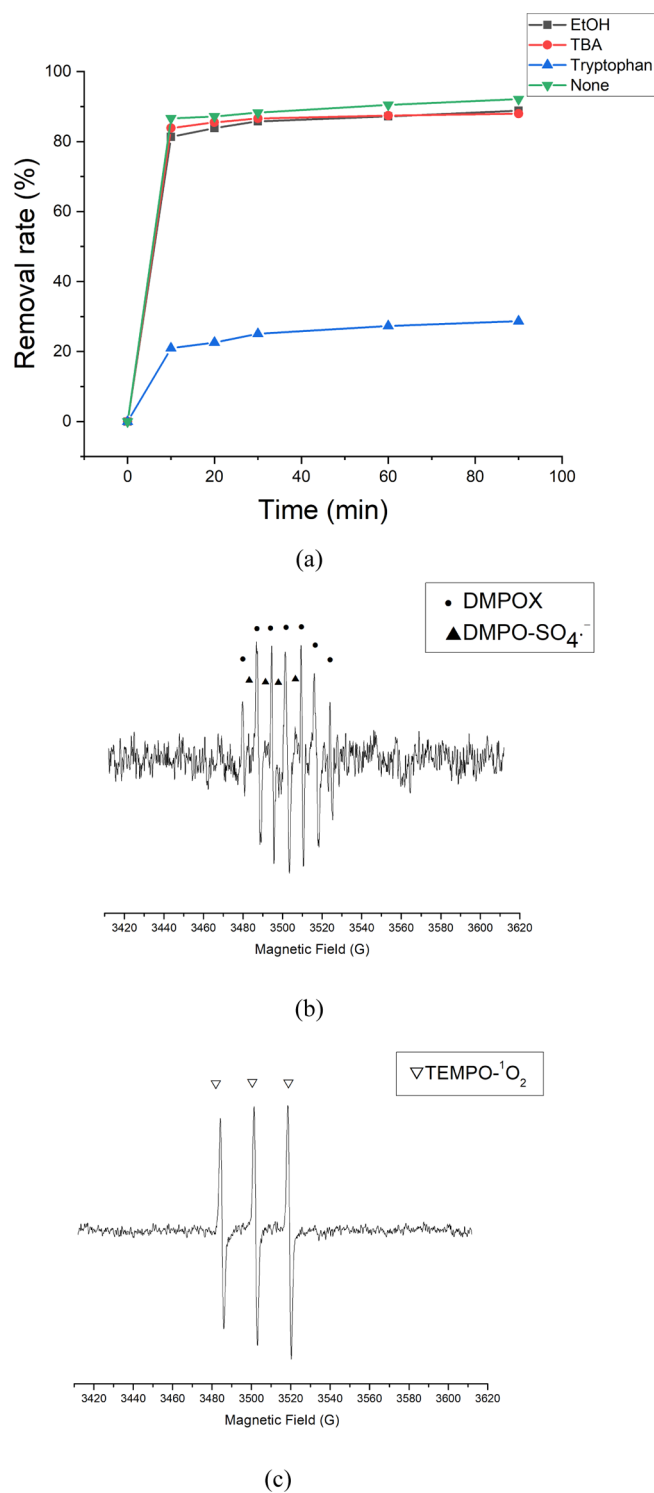

Figure 10. (a) Radical quenching tests; ESR tests for (b) $SO_4^{\bullet-}$, $^{\bullet}OH$, and (c) $^1O_2$.

nm, λ_{em} = 380−540 nm and λ_{ex} = 250−400 nm, λ_{em} = 380−540 nm). The TOC removal rate under optimal conditions was calculated as 52.7%, which indicated the uncompleted minimization of HA. In addition, the leachate concentration of the main metal element in OBDCA-sp was analyzed using ICP-OES (Table 2). The leachate concentration of heavy metals was very low, guaranteeing the safe use of OBDCA-sp in environmental remediation.
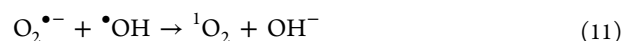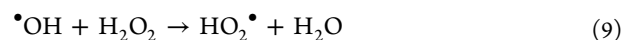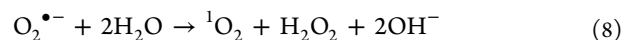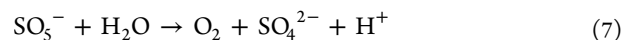
To postulate the potential metal components and elements in OBDCA-sp for PMS activation, characterization by XPS and XRD was done for structural analysis. The XRD pattern of OBDCA-sp (Figure 8) exhibited complex and mass peaks. The diffraction peaks at 2θ = 20.8, 26.6, 36.5, 39.4, and 50.1° were assigned to quartz (SiO_2, PDF 79-1906).[32] The 2θ = 32.9, 55.2, 23.1, 38.2, and 65.8° corresponded to bixbyite ($FeMnO_3$, PDF 75-0894).[33] The characteristic diffraction peaks at 2θ = 23.1, 32.9, 38.2, and 55.1° were ascribed to manganese oxide (Mn_2O_3, PDF 71-0636).[34] The characteristic diffraction peaks at 2θ = 32.9, 38.2, 55.2, and 65.8° were ascribed to iron oxide (Fe_2O_3, PDF 39-0238).[35] The results indicated that the main components of OBDCA-sp were SiO_2, $FeMnO_3$, Mn_2O_3, and Fe_2O_3. The surface element state of OBDCA-sp was analyzed using XPS (Figure 9). Co was detected in the XPS spectra of OBDCA-sp. The corresponding peaks of Co were 780.1 and 795.4 eV. The separation of binding energy between the doublets was 15.3 eV, indicating that the possible value state for the Co element was Co^{3+}. The Co-containing component was not detected in XRD, as the content of Co-containing component was lower than the lower detection limitation of XRD. According to a previous report, the existing form of Co was postulated to be Co_2O_3.[36,37] Two spin orbitals of core-level Fe 2p were detected. Fe $2p_{3/2}$ and Fe $2p_{1/2}$ were located at 711.1 and 724.7 eV, respectively. The spin energy separation between the two spin orbitals was 13.6 eV, indicating that the possible value state for the Fe element was Fe^{3+}.[38] According to the XRD results, the existing form of Fe was postulated to be Fe_2O_3 and $FeMnO_3$. An obvious spin orbital for O 1s was observed at 531.3 eV, which was attributed to adsorbed oxygen, indicating the oxidation state (O^{2-}) of O element. No obvious spin orbital was detected for Mn 2p, and two spin orbitals were detected for Mn 3s. The distance for spin energy separation of the Mn 3s level was 3 eV, which indicated that the possible value state for Mn was Mn^{3+}.[38] According to the XRD results, the existing forms of Mn were speculated to be Mn_2O and $FeMnO_3$.

The XPS and XRD results of fresh OBDCA-sp and used OBDCA-sp had no obvious change, which indicated the stability of OBDCA-sp.

3.6. Radical Quenching Test and ESR Test. The radical quenching tests (Figure 10) were performed to identify the role of ROS in HA removal. $^{\bullet}OH$, $SO_4^{\bullet-}$, and $^1O_2$ were possible ROS for HA removal according to the previous studies.[39−41] To evaluate the contribution of $^{\bullet}OH$, $SO_4^{\bullet-}$, and $^1O_2$ to HA removal, according to the relative report, EtOH was used as a radical quencher for $^{\bullet}OH$ and $SO_4^{\bullet-}$ and TBA was used as radical quencher for $^{\bullet}OH$. Tryptophan was used as a radical quencher for $^1O_2$.[42,43] The results of radical quenching tests indicated that the addition of tryptophan severely inhibited the removal of HA, while EtOH and TBA had only slight inhibition effect for HA removal. According to the effect of the quencher on HA removal, it was concluded that the order of ROS contribution for HA removal was as follows: $^1O_2 \gg SO_4^{\bullet-} \approx {}^{\bullet}OH$, and $^1O_2$ was the dominant ROS for HA removal.

ESR analysis was employed to determine the ROS produced during PMS activation using OBDCA-sp (Figure 10). DMPO was employed as a radical trapping agent for $^{\bullet}OH$ and $SO_4^{\bullet-}$,[44] and $^1O_2$ was trapped by TEMPO.[45] For signals of DMPO-adduct, two group signal peaks, DMPO-$SO_4^{\bullet-}$ and DMPOX, were detected. DMPOX was formed when DMPO was trapped two hydroxyl groups; for signals of TEMPO-adduct, the signal peaks of TEMPO-$^1O_2$ were evident. ESR analysis confirmed

the presence of $^{\bullet}OH$, $SO_4^{\bullet-}$, and $^1O_2$ in the OBDCA-sp/PMS system. However, due to the complex components of OBDCA-sp, the generation pathway of $^{\bullet}OH$, $SO_4^{\bullet-}$, and $^1O_2$ remains unclear. The possible path generation was postulated as follows (formulae 6−11)[25,46]

$$HSO_5^- \rightarrow H^+ + SO_5^{2-} \tag{6}$$

$$SO_5^- + H_2O \rightarrow O_2 + SO_4^{2-} + H^+ \tag{7}$$

$$O_2^{\bullet-} + 2H_2O \rightarrow {}^1O_2 + H_2O_2 + 2OH^- \tag{8}$$

$${}^{\bullet}OH + H_2O_2 \rightarrow HO_2^{\bullet} + H_2O \tag{9}$$

$$HO_2^{\bullet} \rightarrow H^+ + O_2^{\bullet-} \tag{10}$$

$$O_2^{\bullet-} + {}^{\bullet}OH \rightarrow {}^1O_2 + OH^- \tag{11}$$

4. CONCLUSIONS

In this work, OBDCA-sp was used to activate PMS for HA removal. 92% of HA removal efficiency was achieved under optimal experimental conditions. The performance of OBDCA-sp for PMS activation was attributed to Fe(III), Mn(III), and Co(III) elements in OBDCA-sp. The ROS scavenger experiments and ESR spectra demonstrated that $SO_4^{\bullet-}$, $^{\bullet}OH$, and $^1O_2$ were responsible for HA removal and that $^1O_2$ was the dominant ROS for HA removal. The study indicated the promising potential for the application of OBDCA-sp in the catalysis field and organic pollution treatment.

■ AUTHOR INFORMATION

Corresponding Authors

Yi Zhang − State Key Laboratory of Freshwater Ecology and Biotechnology, Institute of Hydrobiology, Chinese Academy of Sciences, Wuhan 430072, P. R. China; ⊙ orcid.org/0000-0003-4441-3504; Email: zhangyi@ihb.ac.cn

Shibin Xia − School of Resources and Environmental Engineering, Wuhan University of Technology, Wuhan 430070, China; ⊙ orcid.org/0000-0003-4599-7898; Email: shibinxia@126.com

Authors

Yuqing Zhao − School of Resources and Environmental Engineering, Wuhan University of Technology, Wuhan 430070, China; College of Ecology and Environment, Hubei Vocational College of Ecological Engineering, Wuhan 430200, P. R. China; State Key Laboratory of Freshwater Ecology and Biotechnology, Institute of Hydrobiology, Chinese Academy of Sciences, Wuhan 430072, P. R. China

Hang Yang − School of Resources and Environmental Engineering, Wuhan University of Technology, Wuhan 430070, China

Jianfa Sun − China Petroleum & Chemical Corporation Jianghan Oilfield, Chongqing 400000, China

Complete contact information is available at:
https://pubs.acs.org/10.1021/acsomega.1c01597

Notes

The authors declare no competing financial interest.

◼ REFERENCES

(1) Hu, G.; Liu, H.; Chen, C.; Hou, H.; Li, J.; Hewage, K.; Sadiq, R. Low-Temperature Thermal Desorption and Secure Landfill for Oil-Based Drill Cuttings Management: Pollution Control, Human Health Risk, and Probabilistic Cost Assessment. *J. Hazard. Mater.* **2021**, *410*, 124570.

(2) Cui, Z.; Luan, X.; Li, S.; Zhao, X.; Lin, Z.; Li, J.; Gao, W.; Zheng, L.; Ma, Z.; Xie, J. Genotoxicity Detection of Oil-Containing Drill Cuttings by Comet Assay Based on a Demersal Marine Fish Mugilogobius Chulae. *Ecotoxicol. Environ. Saf.* **2021**, *208*, 111655.

(3) Xu, T.; Wang, L. a.; Wang, X.; Li, T.; Zhan, X. Heavy Metal Pollution of Oil-Based Drill Cuttings at a Shale Gas Drilling Field in Chongqing, China: A Human Health Risk Assessment for the Workers. *Ecotoxicol. Environ. Saf.* **2018**, *165*, 160−163.

(4) Araka, P. P.; Okparanma, R. N.; Ayotamuno, J. M. Diagnostic Screening of Organic Contaminant Level in Solidified/Stabilized Pre-Treated Oil-Based Drill Cuttings. *Heliyon* **2019**, *5*, No. e02644.

(5) Chen, Z.; Zhou, J.; Chen, Z.; Chen, H.; Chen, Q.; He, C.; Liu, X.; Yuanjian, X. A Laboratory Evaluation of Superheated Steam Extraction Process for Decontamination of Oil-Based Drill Cuttings. *J. Environ. Chem. Eng.* **2018**, *6*, 6691−6699.

(6) Hou, Y.; Qi, S.; You, H.; Huang, Z.; Niu, Q. The Study on Pyrolysis of Oil-Based Drilling Cuttings by Microwave and Electric Heating. *J. Environ. Manage.* **2018**, *228*, 312−318.

(7) Chen, Z.; Zheng, Z.; Li, D.; Chen, H.; Xu, Y. Continuous Supercritical Water Oxidation Treatment of Oil-Based Drill Cuttings Using Municipal Sewage Sludge as Diluent. *J. Hazard. Mater.* **2020**, *384*, 121225.

(8) Ye, Y.; Li, J.; Zhang, Q.; Feng, J.; Zhu, J.; Yin, D. Nanoemulsion for Oil-Contaminated Oil-Based Drill Cuttings Removal in Lab. *Special Issue 5th International Conference Energy Energy and Environmental Engineering ICEEEE 2017*: Xiamen China, 2017; Vol: 42 (29), pp 18734−18740.

(9) Wang, C.-q.; Lin, X.-y.; Mei, X.-d.; Luo, X.-g. Performance of Non-Fired Bricks Containing Oil-Based Drilling Cuttings Pyrolysis Residues of Shale Gas. *J. Clean. Prod.* **2019**, *206*, 282−296.

(10) Wang, C.-q.; Lin, X.-y.; Wang, D.; He, M.; Zhang, S.-l. Utilization of Oil-Based Drilling Cuttings Pyrolysis Residues of Shale Gas for the Preparation of Non-Autoclaved Aerated Concrete. *Constr. Build. Mater.* **2018**, *162*, 359−368.

(11) Wang, C.-q.; Lin, X.-y.; He, M.; Wang, D.; Zhang, S.-l. Environmental Performance, Mechanical and Microstructure Analysis of Concrete Containing Oil-Based Drilling Cuttings Pyrolysis Residues of Shale Gas. *J. Hazard. Mater.* **2017**, *338*, 410−427.

(12) Liuyang, X.; Yang, H.; Huang, S.; Zhang, Y.; Xia, S. Resource Utilization of Secondary Pyrolysis Oil-Based Drilling Cuttings Ash for Removing Cr (VI) Contaminants: Adsorption Properties, Kinetics and Mechanism. *J. Environ. Chem. Eng.* **2020**, *8*, 104474.

(13) Yang, H.; Huang, S.; Zhang, Y.; Zhou, B.; Manzoor Ahmed, S.; Liu, H.; Liu, Y.; He, Y.; Xia, S. Remediation Effect of Cr (VI)-Contaminated Soil by Secondary Pyrolysis Oil-Based Drilling Cuttings Ash. *Chem. Eng. J.* **2020**, *398*, 125473.

(14) Kohantorabi, M.; Moussavi, G.; Giannakis, S. A Review of the Innovations in Metal- and Carbon-Based Catalysts Explored for Heterogeneous Peroxymonosulfate (PMS) Activation, with Focus on Radical vs. Non-Radical Degradation Pathways of Organic Contaminants. *Chem. Eng. J.* **2021**, *411*, 127957.

(15) Guo, R.; Li, Y.; Chen, Y.; Liu, Y.; Niu, B.; Gou, J.; Cheng, X. Efficient Degradation of Sulfamethoxazole by CoCu LDH Composite Membrane Activating Peroxymonosulfate with Decreased Metal Ion Leaching. *Chem. Eng. J.* **2021**, *417*, 127887.

(16) Chen, H.; Xu, Y.; Zhu, K.; Zhang, H. Understanding Oxygen-Deficient La2CuO4-Δperovskite Activated Peroxymonosulfate for Bisphenol A Degradation: The Role of Localized Electron within Oxygen Vacancy. *Appl. Catal., B* **2021**, *284*, 119732.

(17) Rodríguez-Chueca, J.; Barahona-García, E.; Blanco-Gutiérrez, V.; Isidoro-García, L.; Dos santos-García, A. J. Magnetic CoFe2O4 Ferrite for Peroxymonosulfate Activation for Disinfection of Wastewater. *Chem. Eng. J.* **2020**, *398*, 125606.

(18) Peng, Y.; Tong, W.; Xie, Y.; Hu, W.; Li, Y.; Zhang, Y.; Wang, Y. Yeast Biomass-Induced Co2P/Biochar Composite for Sulfonamide Antibiotics Degradation through Peroxymonosulfate Activation. *Environ. Pollut.* **2021**, *268*, 115930.

(19) Guan, Z.-Y.; Kwon, E.; Lee, J.; Lin, Y.-F.; Lin, K.-Y. A. Electrospun Cobalt Ferrite Nanofiber as a Magnetic and Effective Heterogeneous Catalyst for Activating Peroxymonosulfate to Degrade Sulfosalicylic Acid. *Sep. Purif. Technol.* **2021**, *259*, 118163.

(20) Guo, R.; Chen, Y.; Nengzi, L.-c.; Meng, L.; Song, Q.; Gou, J.; Cheng, X. In Situ Preparation of Carbon-Based Cu-Fe Oxide Nanoparticles from CuFe Prussian Blue Analogues for the Photo-Assisted Heterogeneous Peroxymonosulfate Activation Process to Remove Lomefloxacin. *Chem. Eng. J.* **2020**, *398*, 125556.

(21) Guo, J.; Khan, S.; Cho, S.-H.; Kim, J. ZnS Nanoparticles as New Additive for Polyethersulfone Membrane in Humic Acid Filtration. *J. Ind. Eng. Chem.* **2019**, *79*, 71−78.

(22) Lyu, C.; Liu, R.; Li, X.; Song, Y.; Gao, H. Degradation of Dissolved Organic Matter in Effluent of Municipal Wastewater Plant by a Combined Tidal and Subsurface Flow Constructed Wetland. *J. Environ. Sci.* **2021**, *106*, 171−181.

(23) Tian, C.; Li, J.; Li, Q.; Nie, Y.; Tian, X.; Dai, C.; Yang, C.; Zhou, Z.; Wang, Y. Surface Weak Acid-Base Pair of FeOOH/Al2O3 for Enhanced Peroxymonosulfate Activation in Degradation of Humic Substances from Water. *Chem. Eng. J.* **2020**, *387*, 124064.

(24) Zhang, W.; Xie, D.; Li, X.; Ye, W.; Jiang, X.; Wang, Y.; Liang, W. Electrocatalytic Removal of Humic Acid Using Cobalt-Modified Particle Electrodes. *Appl. Catal. Gen.* **2018**, *559*, 75−84.

(25) Jiang, J.; Wang, X.; Zhang, C.; Li, T.; Lin, Y.; Xie, T.; Dong, S. Porous 0D/3D NiCo2O4/g-C3N4 Accelerate Emerging Pollutant Degradation in PMS/Vis System: Degradation Mechanism, Pathway and Toxicity Assessment. *Chem. Eng. J.* **2020**, *397*, 125356.

(26) Chen, G.; Zhang, X.; Gao, Y.; Zhu, G.; Cheng, Q.; Cheng, X. Novel Magnetic MnO2/MnFe2O4 Nanocomposite as a Heterogeneous Catalyst for Activation of Peroxymonosulfate (PMS) toward Oxidation of Organic Pollutants. *Sep. Purif. Technol.* **2019**, *213*, 456−464.

(27) Wang, G.; Zhao, Y.; Ma, H.; Zhang, C.; Dong, X.; Zhang, X. Enhanced Peroxymonosulfate Activation on Dual Active Sites of N Vacancy Modified G-C3N4 under Visible-Light Assistance and Its Selective Removal of Organic Pollutants. *Sci. Total Environ.* **2021**, *756*, 144139.

(28) Zeng, Z.; Khan, A.; Wang, Z.; Zhao, M.; Mo, W.; Chen, Z. Elimination of Atrazine through Radical/Non-Radical Combined Processes by Manganese Nano-Catalysts/PMS and Implications to the Structure-Performance Relationship. *Chem. Eng. J.* **2020**, *397*, 125425.

(29) Xu, H.; Jiang, N.; Wang, D.; Wang, L.; Song, Y.; Chen, Z.; Ma, J.; Zhang, T. Improving PMS Oxidation of Organic Pollutants by Single Cobalt Atom Catalyst through Hybrid Radical and Non-Radical Pathways. *Appl. Catal., B* **2020**, *263*, 118350.

(30) Zhang, W.; He, Y.; Li, C.; Hu, X.; Yang, S.; You, X.; Liang, W. Persulfate Activation Using Co/AC Particle Electrodes and Synergistic Effects on Humic Acid Degradation. *Appl. Catal., B* **2021**, *285*, 119848.

(31) Tuan, D. D.; Hu, C.; Kwon, E.; Du, Y.; Lin, K.-Y. A. Coordination Polymer-Derived Porous Co3O4 Nanosheet as an Effective Catalyst for Activating Peroxymonosulfate to Degrade Sulfosalicylic Acid. *Appl. Surf. Sci.* **2020**, *532*, 147382.

(32) Pei, D.; Li, Y.; Cang, D. In Situ XRD Study on Sintering Mechanism of SiO2-Al2O3-CaO-MgO Ceramics from Red Mud. *Mater. Lett.* **2019**, *240*, 229−232.

(33) Ryabova, A. S.; Istomin, S. Y.; Dosaev, K. A.; Bonnefont, A.; Hadermann, J.; Arkharova, N. A.; Orekhov, A. S.; Sena, R. P.; Saveleva, V. A.; Kéranguéven, G.; Antipov, E. V.; Savinova, E. R.; Tsirlina, G. A. Mn2O3 Oxide with Bixbyite Structure for the Electrochemical Oxygen Reduction Reaction in Alkaline Media: Highly Active If Properly Manipulated. *Electrochim. Acta* **2021**, *367*, 137378.

(34) Amsaveni, P.; Nivetha, A.; Sakthivel, C.; Suresh Philip, C.; Prabha, I. Effectiveness of Surfactants for Unique Hierarchical Mn2O3 Nanomaterials as Enhanced Oxidative Catalysts, Antibacterial Agents, and Photocatalysts. *J. Phys. Chem. Solids* **2020**, *144*, 109429.

(35) Wang, H.-m.; Ma, Y.-p.; Chen, X.-y.; Xu, S.-y.; Chen, J.-d.; Zhang, Q.-l.; Zhao, B.; Ning, P. Promoting Effect of SO2−4 Functionalization on the Performance of Fe2O3 Catalyst in the Selective Catalytic Reduction of NOx with NH3. *J. Fuel Chem. Technol.* **2020**, *48*, 584−593.

(36) Kanakkillam, S. S.; Krishnan, B.; Avellaneda, D. A.; Shaji, S. Surfactant Free Stable Cobalt Oxide Nanocolloid in Water by Pulsed Laser Fragmentation and Its Thin Films for Visible Light Photocatalysis. *Colloids Surf., A* **2020**, *594*, 124657.

(37) Warang, T.; Patel, N.; Fernandes, R.; Bazzanella, N.; Miotello, A. Co3O4 Nanoparticles Assembled Coatings Synthesized by Different Techniques for Photo-Degradation of Methylene Blue Dye. *Appl. Catal., B* **2013**, *132-133*, 204−211.

(38) Alam, M. M.; Rahman, M. M.; Uddin, M. T.; Asiri, A. M.; Uddin, J.; Islam, M. A. Fabrication of Enzyme-Less Folic Acid Sensor Probe Based on Facile Ternary Doped Fe2O3/NiO/Mn2O3 Nanoparticles. *Curr. Res. Biotechnol.* **2020**, *2*, 176−186.

(39) Cheng, C.; Gao, S.; Zhu, J.; Wang, G.; Wang, L.; Xia, X. Enhanced Performance of LaFeO3 Perovskite for Peroxymonosulfate Activation through Strontium Doping towards 2,4-D Degradation. *Chem. Eng. J.* **2020**, *384*, 123377.

(40) Chen, Z.; Wang, L.; Xu, H.; Wen, Q. Efficient Heterogeneous Activation of Peroxymonosulfate by Modified CuFe2O4 for Degradation of Tetrabromobisphenol A. *Chem. Eng. J.* **2020**, *389*, 124345.

(41) Li, W.; Zhang, Y.; Liu, Y.; Cheng, X.; Tang, W.; Zhao, C.; Guo, H. Kinetic Performance of Peroxymonosulfate Activated by Co/Bi25FeO40: Radical and Non-Radical Mechanism. *J. Taiwan Inst. Chem. Eng.* **2019**, *100*, 56−64.

(42) Li, Y.; Pan, L.; Zhu, Y.; Yu, Y.; Wang, D.; Yang, G.; Yuan, X.; Liu, X.; Li, H.; Zhang, J. How Does Zero Valent Iron Activating Peroxydisulfate Improve the Dewatering of Anaerobically Digested Sludge? *Water Res.* **2019**, *163*, 114912.

(43) Yang, J.; Liu, X.; Wang, D.; Xu, Q.; Yang, Q.; Zeng, G.; Li, X.; Liu, Y.; Gong, J.; Ye, J.; Li, H. Mechanisms of Peroxymonosulfate Pretreatment Enhancing Production of Short-Chain Fatty Acids from Waste Activated Sludge. *Water Res.* **2019**, *148*, 239−249.

(44) Liu, N.; Lu, N.; Yu, H.; Chen, S.; Quan, X. Degradation of Aqueous Bisphenol A in the CoCN/Vis/PMS System: Catalyst Design, Reaction Kinetic and Mechanism Analysis. *Chem. Eng. J.* **2021**, *407*, 127228.

(45) Peng, G.; You, W.; Zhou, W.; Zhou, G.; Qi, C.; Hu, Y. Activation of Peroxymonosulfate by Phosphite: Kinetics and Mechanism for the Removal of Organic Pollutants. *Chemosphere* **2021**, *266*, 129016.

(46) Huang, Z.; Wu, P.; Liu, C.; Chen, M.; Yang, S.; Dang, Z.; Zhu, N. Multiple Catalytic Reaction Sites Induced Non-Radical/Radical Pathway with Graphene Layers Encapsulated Fe-N-C toward Highly Efficient Peroxymonosulfate (PMS) Activation. *Chem. Eng. J.* **2021**, *413*, 127507.